

CONVOLUTIONAL NEURAL NETWORK-BASED EFFICIENT DENSE POINT CLOUD GENERATION USING UNSIGNED DISTANCE FIELDS

Abol Basher and Jani Boutellier

School of Technology and Innovation
University of Vaasa
Vaasa, Finland

ABSTRACT

Dense point cloud generation from a sparse or incomplete point cloud is a crucial and challenging problem in 3D computer vision and computer graphics. So far, the existing methods are either computationally too expensive, suffer from limited resolution, or both. In addition, some methods are strictly limited to watertight surfaces — another major obstacle for a number of applications. To address these issues, we propose a lightweight Convolutional Neural Network that learns and predicts the unsigned distance field for arbitrary 3D shapes for dense point cloud generation using the recently emerged concept of implicit function learning. Experiments demonstrate that the proposed architecture outperforms the state of the art by 87% less model parameters, 36% reduced inference time and improved generated point cloud accuracy.

Index Terms— Point cloud, implicit representation, CNN, unsigned distance field, 3D reconstruction

1. INTRODUCTION

With the advances and wider availability of real-time 3D sensors such as LiDAR and depth cameras, 3D data (e.g., point clouds) have received increased popularity in computer vision and robotics. However, the point clouds acquired from 3D sensors are often incomplete or sparsely distributed because of occlusion or sensor resolution limitations. Recovering the complete shape/structure or generating dense point clouds is a challenging task in 3D computer vision [1], and moreover, for many applications, it is useful to have a continuous surface representation. Although several works [2, 3, 4] have focused on image-based 3D shape reconstruction, in this study, we concentrate on dense point cloud generation from a sparse (possibly incomplete) point cloud.

The conventional data types representing 3D geometry include voxels, point clouds, and meshes, each with their own limitations: voxel-based representations [4] have a large memory footprint, which limits the output resolution; point

cloud-based representations [5] are disconnected and trivially do not allow rendering and visualization of the surface; and meshes [6] are limited to a single topology and can have issues related to continuity.

Recently emerged *implicit representations* of 3D shapes or surfaces attempt to address these limitations. Although implicit representation based approaches [7, 8, 9, 10] are conceptually similar, they differ in inference and shape representation (occupancy values, signed/unsigned distances). The implicit function learning based approaches, which use occupancy values or signed distances as ground truths, require closed surfaces, and can obtain the final shape/surface in the form of a mesh through post-processing. However, in the case of occupancy values or signed distances, it is often hard to express a shape in terms of 'inside' and 'outside' (e.g., hollow objects or 3D scenes). Fortunately, recently *unsigned distance* based implicit approaches have emerged, not suffering from the requirement of closed surfaces.

In implicit representation, a 3D shape/surface \mathcal{S} is expressed as a (zero) level set (Equation 1)

$$\mathcal{S} = \{p \in \mathbb{R}^3 | f(p, z) = t\}, \quad (1)$$

where $z \in \mathbb{Z} \subset \mathbb{R}^m$ is a latent code representing a 3D shape, $p \in \mathbb{R}^3$ is a query point in 3D space, and t is the threshold parameter (if $t = 0$, then Equation 1 is known as zero level set). For implicit 3D shape/surface representation, a (convolutional) neural network $f(\cdot)$ is trained to learn the continuous points in 3D space and predict an occupancy $f(p, z) : \mathbb{R}^3 \times \mathbb{Z} \rightarrow [1, 0]$, signed distance $f(p, z) : \mathbb{R}^3 \times \mathbb{Z} \rightarrow \mathbb{R}$, or unsigned distance $f(p, z) : \mathbb{R}^3 \times \mathbb{Z} \rightarrow \mathbb{R}_0^+$.

Most recent implicit representation-based works [7, 10, 11] encode a 3D shape/surface using a single latent vector z and obtain a continuous presentation of the surface by learning a neural function. Due to encoding the complete shape into a single latent code, those models are prone to lose details present in the data and the original alignment [8] of the shape embedding in 3D space. Recently, two novel approaches have been proposed to address those limitations – If-Nets [8] and neural distance fields (NDF) [9]. These methods encode an input shape/surface into multi-scale multi-level deep features

This work has been partially supported by the Academy of Finland projects CoEfNet and REPEAT.

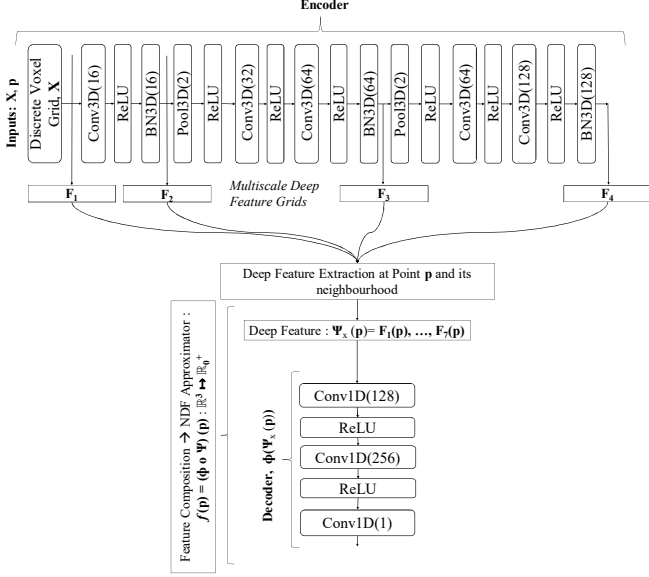


Fig. 1. Proposed LightNDF architecture. Here, $\mathbf{X} \in \mathcal{X}$ is input data to the encoder, while $\mathcal{X} = \mathbb{R}^{N \times N \times N}$ is a discrete voxel grid, N is the input resolution, and \mathbf{p} is a query point.

and use these to decode the continuous shape/surface. However, NDF [9] relies on a convolutional neural network architecture that contains 4.6 million trainable parameters. In this study, we propose a lightweight (0.6 million parameter) convolutional neural network architecture, *LightNDF*¹, which relies on neural unsigned distance fields for implicit 3D shape representation. Compared to the state-of-the-art NDF architecture [9], LightNDF

- Has $7.6\times$ less model parameters,
- 36% reduced inference time, and 19% reduced training time, while
- Outperforming NDF in generated point cloud quality.

We regard the significant reduction of neural architecture size, and the reduced inference time as important factors towards wider adoption of neural implicit methods for 3D shape completion and point cloud densification.

2. RELATED WORK

In the following, a brief review on related work in 3D representations is presented.

2.1. Traditional representations

Traditional 3D data representations include: (a) voxels, (b) point clouds, and (c) meshes. *Voxel*-based representations (e.g., [12]) are commonly used for shape/surface learning.

The convolution operation can naturally be applied to voxels, however, memory footprints increase cubically with the resolution limiting the ability of voxels to handle higher resolutions. Several works have proposed solutions to this memory issue [13, 14]. The *point cloud* representation [5, 15] is another popular choice and is the output format of many sensors, e.g., LiDAR and depth cameras. The pioneering research work PointNet [5] has recently popularized the point cloud-based research for discriminative learning. However, due to having no connectivity information, point clouds are not well-suited for generating watertight surfaces [11]. *Mesh*-based representations [16, 17] are a more informative data type and offer connectivity information between 3D points. By deforming a template, 3D shape can be inferred using mesh-based approaches; therefore, mesh-based methods are limited to a single topological representation [18, 6].

2.2. Implicit representation

Recently emerged implicit function learning-based works [9, 8, 7, 19, 10] have shown success in 3D shape representation, completion, and reconstruction. These presentations work based on zero level sets of a function (see Equation 1) and learn either binary occupancy values [10] or signed/unsigned distance functions/fields [9, 8, 19]. Implicit representations can represent shape and scene in a continuous fashion with various topologies. However, one important drawback of these methods, which rely on occupancy or signed distance, is that they require watertight shapes or scenes, which are not always available. Recently proposed neural unsigned distance fields (NDF) [9] have addressed these issues and can represent wider classes of surfaces, mathematical functions, and manifolds; unfortunately, this recently proposed approach is computationally complex. For addressing this issue, in the following we present a compact neural network architecture for unsigned distance field learning and inference.

3. PROPOSED NETWORK

In the following, we present our lightweight convolutional neural network architecture, *LightNDF* for implicit representation of the 3D geometry, inspired by the literature [20, 8]. Here, we describe how the proposed LightNDF architecture learns to encode and decode a 3D shape/surface, along with the training and inference details.

3.1. Encoder

The LightNDF encoder is based on a 3D convolutional neural network (CNN) similar to the NDF encoder, to handle the discrete 3D voxel grid $\mathcal{X} = \mathbb{R}^{N \times N \times N}$ generated from a sparse point cloud, $\mathbf{X} \in \mathcal{X}$ of an object; however, the trainable parameter count of the LightNDF encoder is about

¹Source code available at: <https://github.com/basher8488881/LightNDF>

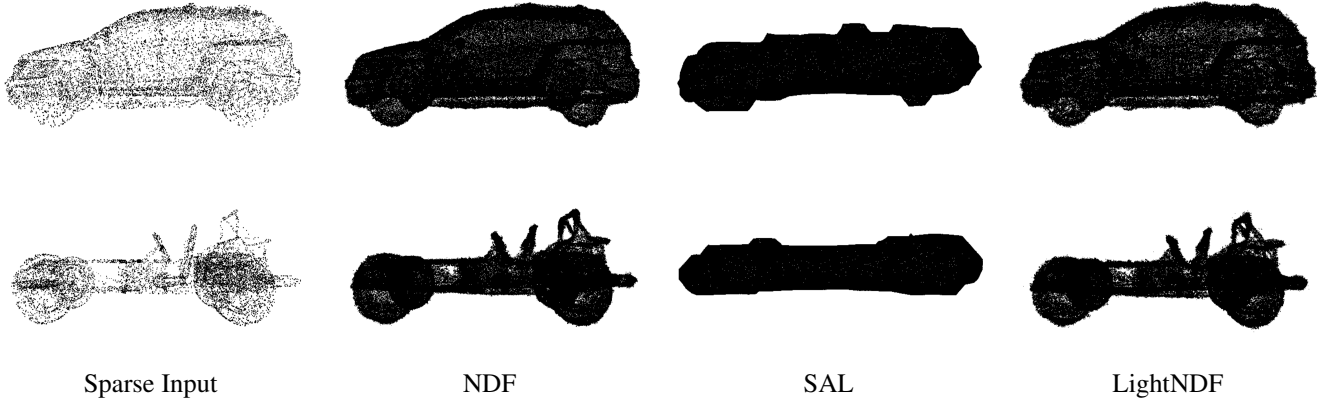


Fig. 2. The generated dense 1M point clouds (from left to right): Sparse input (10,000 points), NDF (baseline), SAL, LightNDF (proposed). Due to the hollow input shape, SAL has significant difficulties in shape generation. Point cloud details are better visible when zoomed-in.

$7.4\times$ smaller compared to baseline NDF. Instead of generating a single latent code of input data like other implicit representation-based approaches, LightNDF encodes the input shape using the 3D CNN into multi-scale deep feature grids $\mathbf{F}_1, \dots, \mathbf{F}_n, \mathbf{F}_k \in \mathcal{F}^{K \times K \times K}$, with the resolution K decreasing by factor of 2^{k-1} and $\mathcal{F}_k \in \mathbb{R}^C$ being a multi-channel feature where C is the number of channels. In the early stages, the extracted features \mathcal{F}_k (starting at $k = 1$) capture local detail of the shape, whereas the higher-level features (ending at $k = n$; in the case of LightNDF, $n = 4$) capture the global structure of input data by utilizing larger receptive fields. To some extent our encoder resembles one of the six-layer If-Net [8] variants used to extract deep feature grids for voxel-grid reconstruction (super-resolution) from 32^3 resolution; however, our proposed LightNDF encoder has five convolutional layers with significantly different filter configurations, and is used to extract deep feature grids with a resolution of 256^3 . This multi-scale feature extraction process enables the encoder to reason about sparse data and retain the input data details. The encoder architecture with the filter settings in each layer is shown in Fig. 1.

3.2. Decoder

The LightNDF decoder (see Fig. 1) consists of three 1D convolutional layers, with the first two layers followed by a ReLU non-linear activation function. The LightNDF decoder filter setting is in the pattern of $(128 \rightarrow 256 \rightarrow 1)$, whereas baseline NDF has four 1D convolutional layers and the filter setting pattern is $(512 \rightarrow 256 \rightarrow 256 \rightarrow 1)$.

From the multi scale deep feature grids, a neural function, $\Psi(\mathbf{p}) = \mathbf{F}_1(\mathbf{p}), \dots, \mathbf{F}_n(\mathbf{p})$, extracts deep features using trilinear interpolation at the location of a query point $\mathbf{p} \in \mathbb{R}^3$ and its neighborhood. The extracted deep features $\mathbf{F}_1(\mathbf{p}), \dots, \mathbf{F}_n(\mathbf{p})$ are fed to the decoder $\Phi(\mathbf{F}_1(\mathbf{p}), \dots, \mathbf{F}_n(\mathbf{p}))$,

which then predicts the unsigned distance function (UDF) to the ground truth surface, $\text{UDF}(\mathbf{p}, \mathcal{S}) = \min_{\mathbf{q} \in \mathcal{S}} \|\mathbf{p} - \mathbf{q}\|$, from the deep features, where \mathbf{q} is the closest surface point from \mathbf{p} . Therefore, the LightNDF or NDF approximator $f(\mathbf{p})$, which approximates the points to unsigned distance, is obtained by composition and can be expressed by Equation 2:

$$f(\mathbf{p}) = (\Phi \circ \Psi)(\mathbf{p}) : \mathbb{R}^3 \longrightarrow \mathbb{R}_0^+. \quad (2)$$

3.3. Model training

Training samples for the proposed model are generated by sampling points $\mathbf{p} \in \mathbb{R}^3$ close to surface \mathcal{S} (provided in mesh format for our dataset) and by computing the corresponding ground truth $\text{UDF}(\mathbf{p}, \mathcal{S})$ using clamped regressed distance (10 cm) to learn distances. The proposed LightNDF and NDF $f(p)$ encoder and decoder were parameterized by neural weights \mathbf{w} and trained jointly via mini-batch loss with the Adam optimizer [21] and mean absolute error loss function (L1 loss); the learning rate was 0.000001. Both the proposed LightNDF and the baseline NDF model are implemented in PyTorch and were allowed to train for 50 epochs on a dual 24-GB Geforce RTX 3090 GPU, however the models converged already by 40 epochs. The proposed architecture was somewhat faster to train than the baseline, as the duration for a LightNDF training epoch was around 14.1 minutes, whereas for baseline NDF a training epoch took 17.4 minutes.

3.4. Inference and dense point cloud generation

In the inference phase both the LightNDF and the baseline NDF model generate a complete UDF surface given a sparse point cloud. The surface can then be used to generate a dense point cloud, or a mesh. We used visualization Algorithm 1 of [9] to extract the dense point cloud from predicted UDFs. If the proposed LightNDF or baseline NDF approximator $f(\mathbf{p})$

perfectly estimates the true $\text{UDF}(\mathbf{p})$, then a point \mathbf{p} can be projected to the nearest surface point \mathbf{q} by moving in the negative gradient direction using visualization Algorithm 1 [9]. Repeating the projection [9] multiple times ($5\times$ in our experiments) generates millions of points on the surface. Dense point clouds can be used in many applications, such as point-based modeling [22], and for learning shape representations such as point cloud-based segmentation and classification [5].

4. EXPERIMENTAL RESULTS

This section presents the dataset, baseline, and performance evaluation for the proposed LightNDF architecture.

4.1. Dataset and baselines

The ShapeNet dataset [23] consists of classes of rigid objects — for example, cars, lamps, chairs, tables, and planes, containing more than 3,000,000 models. The ShapeNetCore subset used in this work contains 51,300 unique 3D models belonging to 55 categories, where each of the models is manually verified, with alignment annotations provided. In this work, we use the Cars subset of ShapeNetCore: from the 3514 models of the Car class, about 70% (2461) were used to train the model, 20% (702) for testing, and 10% (351) for validation. Using this data, the models were used to perform *reconstruction of previously unseen shapes*, i.e. learning from the training set, and generating dense point clouds from the sparse samples of the test set.

The NDF neural network architecture proposed in [9], and Sign Agnostic Learning (SAL) [7] were used as the baseline for evaluating LightNDF performance. We compared our LightNDF architecture against NDF [9] and SAL for the task of dense point cloud generation from sparse point clouds. Each architecture was trained on our own workstations using the same training and test data splits.

4.2. Performance and comparison

Quantitative comparison between the trained models was performed using the Chamfer- L_2 distance metric, where lower values are better, and zero means a full match between the generated point cloud and the ground truth. The results are shown for 3000 and 10000 input points in Table 1 (in the scale of $\times 10^{-4}$). It can be seen from the Chamfer- L_2 distance that quantitatively the proposed LightNDF model slightly outperforms baseline NDF, but SAL [7] with a significant margin, in previously unseen shape generation.

In Fig. 2, a visual comparison of dense point clouds generated by the proposed LightNDF architecture and the baseline NDF for 10000 input points are shown, for 1M generated points. Observation of the generated dense point clouds reveals no significant differences between NDF and LightNDF, whereas the other baseline approach, SAL, shows inferior

Table 1. Model comparison. Chamfer- L_2 ($\text{CD-}L_2$) distances measure the accuracy and completeness of the surface between the dense point clouds (generated by LightNDF, SAL and NDF) and the ground truth, for 10000 and 3000 input points. $\text{CD-}L_2$ results are reported in the scale of $\times 10^{-4}$. Projection times are for 5 projection steps. *For all measures, lower values are better.*

Model	# Trainable Parameters	$\text{CD-}L_2$ 10000	$\text{CD-}L_2$ 3000	Proj. time 10000	Proj. time 3000
NDF [9]	4.6M	0.242	0.325	4.642 s	4.633 s
SAL [7]	4.2M	7.444	9.170	-	-
LightNDF (Proposed)	0.6M	0.231	0.309	2.970 s	2.976 s

quality due to its inability to handle hollow shapes. Table 1 also shows the projection (inference) times for the different models, revealing that the significantly smaller LightNDF architecture takes 36% less time in inference compared to NDF. All presented values are an average over the 702 test shapes.

It was observed that the number of initial sample points \mathbf{p} (see Section 3.4) has a significant impact to inference time for both the baseline NDF and the proposed LightNDF model. Inference time-optimal values of \mathbf{p} were identified to be 20100 for baseline NDF and 5050 for LightNDF; Table 1 results are for these values of \mathbf{p} . The value of \mathbf{p} had a negligible impact on generated point cloud quality for LightNDF; however for baseline NDF somewhat better quality could be achieved by increasing \mathbf{p} up to 201000. By using this value of \mathbf{p} , Chamfer- L_2 values of 0.234×10^{-4} (10000 points) and 0.319×10^{-4} (3000 points) were achieved for baseline NDF, however increasing the inference time to 6.616 s, which is $2.23\times$ the inference time of the proposed LightNDF model.

5. DISCUSSION AND CONCLUSION

In this work, we introduced the LightNDF neural network architecture for dense point cloud generation. The proposed architecture significantly outperforms the state-of-the-art NDF architecture in terms of model parameter count, and also provides slightly better quality of generated dense point clouds. Smaller model size reduces inference time by 36%, which we regard as an important development towards wider adoption of neural implicit models for 3D point cloud completion and densification. As future work we plan to study means for reducing computation time of the 3D convolutions present in the LightNDF encoder.

6. REFERENCES

- [1] Tianxin Huang, Hao Zou, Jinhao Cui, Xueming Yang, Mengmeng Wang, Xiangrui Zhao, Jiangning Zhang, Yi Yuan, Yifan Xu, and Yong Liu, “RFNet: Recurrent

- forward network for dense point cloud completion,” in *IEEE/CVF International Conference on Computer Vision*, 2021.
- [2] Priyanka Mandikal and Venkatesh Babu Radhakrishnan, “Dense 3d point cloud reconstruction using a deep pyramid network,” in *IEEE Winter Conference on Applications of Computer Vision*. IEEE, 2019.
 - [3] Minghua Liu, Lu Sheng, Sheng Yang, Jing Shao, and Shi-Min Hu, “Morphing and sampling network for dense point cloud completion,” in *AAAI Conference on Artificial Intelligence*, 2020, vol. 34.
 - [4] Christopher B Choy, Danfei Xu, JunYoung Gwak, Kevin Chen, and Silvio Savarese, “3D-R2N2: A unified approach for single and multi-view 3D object reconstruction,” in *European Conference on Computer Vision*. Springer, 2016, pp. 628–644.
 - [5] Charles R Qi, Hao Su, Kaichun Mo, and Leonidas J Guibas, “PointNet: Deep learning on point sets for 3D classification and segmentation,” in *IEEE Conference on Computer Vision and Pattern Recognition*, 2017.
 - [6] Nanyang Wang, Yinda Zhang, Zhuwen Li, Yanwei Fu, Wei Liu, and Yu-Gang Jiang, “Pixel2mesh: Generating 3D mesh models from single RGB images,” in *European Conference on Computer Vision*, 2018, pp. 52–67.
 - [7] Matan Atzmon and Yaron Lipman, “SAL: Sign agnostic learning of shapes from raw data,” in *IEEE/CVF Conference on Computer Vision and Pattern Recognition*, 2020.
 - [8] Julian Chibane and Gerard Pons-Moll, “Implicit feature networks for texture completion from partial 3D data,” in *European Conference on Computer Vision*. Springer, 2020, pp. 717–725.
 - [9] Julian Chibane, Aymen Mir, and Gerard Pons-Moll, “Neural unsigned distance fields for implicit function learning,” in *Advances in Neural Information Processing Systems*, December 2020.
 - [10] Lars Mescheder, Michael Oechsle, Michael Niemeyer, Sebastian Nowozin, and Andreas Geiger, “Occupancy networks: Learning 3D reconstruction in function space,” in *IEEE Conference on Computer Vision and Pattern Recognition*, 2019.
 - [11] Jeong Joon Park, Peter Florence, Julian Straub, Richard Newcombe, and Steven Lovegrove, “DeepSDF: Learning continuous signed distance functions for shape representation,” in *IEEE Conference on Computer Vision and Pattern Recognition*, 2019, pp. 165–174.
 - [12] Zerong Zheng, Tao Yu, Yixuan Wei, Qionghai Dai, and Yebin Liu, “DeepHuman: 3D human reconstruction from a single image,” in *IEEE International Conference on Computer Vision*, 2019, pp. 7739–7749.
 - [13] Maxim Tatarchenko, Alexey Dosovitskiy, and Thomas Brox, “Octree generating networks: Efficient convolutional architectures for high-resolution 3D outputs,” in *IEEE International Conference on Computer Vision*, 2017, pp. 2088–2096.
 - [14] Christian Häne, Shubham Tulsiani, and Jitendra Malik, “Hierarchical surface prediction for 3D object reconstruction,” in *International Conference on 3D Vision*. IEEE, 2017, pp. 412–420.
 - [15] Sergey Prokudin, Christoph Lassner, and Javier Romero, “Efficient learning on point clouds with basis point sets,” in *IEEE International Conference on Computer Vision Workshops*, 2019.
 - [16] Pengyu Wang, Yuan Gan, Panpan Shui, Fenggen Yu, Yan Zhang, Songle Chen, and Zhengxing Sun, “3d shape segmentation via shape fully convolutional networks,” *Computers & Graphics*, vol. 70, 2018.
 - [17] Anurag Ranjan, Timo Bolkart, Soubhik Sanyal, and Michael J Black, “Generating 3D faces using convolutional mesh autoencoders,” in *European Conference on Computer Vision*, 2018, pp. 704–720.
 - [18] Chen-Hsuan Lin, Oliver Wang, Bryan C Russell, Eli Shechtman, Vladimir G Kim, Matthew Fisher, and Simon Lucey, “Photometric mesh optimization for video-aligned 3D object reconstruction,” in *IEEE Conference on Computer Vision and Pattern Recognition*, 2019.
 - [19] Matan Atzmon and Yaron Lipman, “SALD: Sign agnostic learning with derivatives,” in *International Conference on Learning Representations*, 2021.
 - [20] Abol Basher, Muhammad Sarmad, and Jani Boutellier, “LightSAL: Lightweight sign agnostic learning for implicit surface representation,” *arXiv preprint arXiv:2103.14273*, 2021.
 - [21] Diederik P Kingma and Jimmy Ba, “Adam: A method for stochastic optimization,” *arXiv preprint arXiv:1412.6980*, 2014.
 - [22] Marc Alexa, Johannes Behr, Daniel Cohen-Or, Shachar Fleishman, David Levin, and Claudio T Silva, “Point set surfaces,” in *Proceedings Visualization, 2001. VIS’01*. IEEE, 2001, pp. 21–29.
 - [23] Angel X Chang et al., “ShapeNet: An information-rich 3D model repository,” *arXiv preprint arXiv:1512.03012*, 2015.